Supporting Information

Bai et al. 10.1073/pnas.1301814110

SI Text

Method for Binding Free Energy Calculation. The molecular mechanic-generalized Born surface area (MM-GBSA) approach combines molecular mechanics, the generalized Born model, and the solvent accessibility method to calculate the binding free energy of a ligand binding to a protein or other macromolecule (receptor) on the basis of the 3D structure of the ligand–receptor complex. The pair-wise generalized Born surface area (GBSA) model has been widely applied and validated in several cases since it was proposed by Still and coworkers (1, 2). However, application of this GBSA model in drug design is limited due to its expensive computational cost (3–5). Although the proposed grid-based GBSA model shows great improvement in computational speed (3, 4), its use is still confined to receptor-rigid simulations. Similarly, a molecular mechanics (MM) model has also been designed as a pair-wise–based and a rigid-based method for energy calculation at high speed (6, 7).

To consider both the flexibility of the receptor and computing speed, we developed an improved MM-GBSA method for predicting ligand–receptor binding free energy. Our method adopts a hybrid MM-GBSA model of pair-wise and grid-based models, which calculates ligand and surrounding flexible residues (core part) by using pair-wise models and computes the other part of the receptor using grid-based models for both MM and GBSA. Thus, our hybrid model may take into account the flexibility of ligand–receptor binding by simulating the core part with the pair-wise model and speed up the computing time by calculating the remaining part with the rigid model.

As mentioned in the main text, the predicting results of the traditional MM-GBSA approaches are not stable enough; for some cases the results are quite promising (RMS errors under 3 kcal/mol), but for many systems the calculations with larger errors have been seen. To enhance the prediction accuracy, we improved the energy function of MM-GBSA by weighting the energy terms with coefficients; thus the energy function can be rewritten as

$$\Delta G_{\text{binding}}^0 = \omega_1 \Delta E_{\text{vdw}} + \omega_2 \Delta E_{\text{es}} + \omega_3 \Delta G_{\text{gb}} + \omega_4 \Delta G_{\text{sa}}, \quad \text{[S1]}$$

where ΔE_{vdw} and ΔE_{es} are, respectively, the van der Waals interaction energy and electrostatic interaction energy, and ΔG_{gb} and ΔG_{sa} refer to the polarization and nonpolarization components of salvation free energy, respectively. Weighting factors ω_1–ω_4 can be obtained by fitting the experimental binding free energies of a series of existing ligands to the receptor with the multiple linear regression method. It should be noted that we have regrouped the components of the energy terms by integrating the electrostatic portion of ΔG_{gb} into ΔE_{es}. Therefore, all four terms of Eq. **S1** are independent and will not mutually interfere during docking simulation by using these terms as optimization objectives (*Molecular Docking for Binding Configurations Sampling* section). In addition, we considered the energy penalties from the conformational changes for ligand and receptor. Thus, the four MM-GBSA terms are given by

$$\Delta E_{\text{vdw}} = \Delta E_{\text{vdw,RL}} + \Delta E_{\text{vdw,L}}^{\text{conf}} + \Delta E_{\text{vdw,R}}^{\text{conf}} \quad \text{[S2]}$$

$$\Delta E_{\text{es}} = \Delta E_{\text{es,RL}} + \Delta E_{\text{es,L}}^{\text{conf}} + \Delta E_{\text{es,R}}^{\text{conf}} \quad \text{[S3]}$$

$$\Delta G_{\text{gb}} = \Delta G_{\text{POL}} + \Delta G_{\text{pol,R}}^{\text{conf}} = \left(G_{\text{pol,RL}} - G_{\text{pol,R}} - G_{\text{pol,L}} \right) + \Delta G_{\text{pol,R}}^{\text{conf}} \quad \text{[S4]}$$

$$\Delta G_{\text{sa}} = \left[\sigma_1 \Delta \left(SA_{\text{hp}} \right) - \sigma_2 \Delta (SA) \right] + \left[\sigma_1 \Delta \left(SA_{\text{hp}}^{\text{conf}} \right) - \sigma_2 \Delta \left(SA^{\text{conf}} \right) \right], \quad \text{[S5]}$$

where RL, R, and L represent ligand–receptor complex, receptor, and ligand, respectively. ΔE_{vdw} and ΔE_{es} are calculated using the Lennard–Jones 6–12 potential and the Coulombic potential, respectively. ΔG_{gb} is calculated using the generalized Born (GB) model, and ΔG_{sa} is computed using the solvent accessibility (SA) model. $\Delta(SA)$ and $\Delta(SA_{\text{hp}})$ are, respectively, the changes for total and hydrophobic solvent accessible surfaces of receptor due to ligand binding. $\Delta E_{\text{vdw,R}}^{\text{conf}}$ ($\Delta E_{\text{es,R}}^{\text{conf}}$) and $\Delta E_{\text{vdw,L}}^{\text{conf}}$ ($\Delta E_{\text{es,L}}^{\text{conf}}$) are the conformational energy penalties for hydrophobic (electrostatic) interactions of receptor and ligand in the complex relative to their reference conformations (e.g., the structure of *apo*-receptor and lowest-energy conformation of ligand in solution), respectively. Correspondingly, $\Delta G_{\text{pol,R}}^{\text{conf}}$, $\Delta(SA_{\text{hp}}^{\text{conf}})$, and $\Delta(SA^{\text{conf}})$ are the energy penalties for solvation free energies from polarization and solvent accessibility due to conformational change of receptor induced by ligand binding. The scaled coefficient parameters in Eq. **S5** were selected as $\sigma_1 = 0.025$ and $\sigma_2 = 0.015$ according to a previous study (3).

Preparation for Input Structures. The X-ray crystal structure of the *apo-Tc*AChE [Protein Data Bank (PDB) ID: 1EA5] was used as the starting structure for sampling binding modes of (−)−Huperzine A (HupA) to *Torpedo californica* acetylcholinesterase (*Tc*AChE). The HupA was protonated by using the *Epik* module encoded in Maestro (8) and its atomic partial charge was assigned by means of the Gasteiger–Marsili method (9). The structure of *Tc*AChE was prepared by using Sybyl 6.8 (10) and parameterized according to the Amber ff99 force field (11). For docking simulations and binding free energy calculations, the flexible residues surrounding the active gorge of *Tc*AChE were identified by comparing a series of X-ray crystal structures of apo-*Tc*AChE and inhibitor-*Tc*AChE complexes (PDB IDs: 1E66, 1EA5, 1EVE, 1GPK, 1GPN, 1GQR, 1H22, 1H23, 1HBJ, 1ODC, 1U65, 1UT6, 1VXO, 1VXR, 1W4L, 1W6R, 1W75, 1W76, 1ZGB, 1ZGC, 2BAG, 2C4H, 2C5F, 2C5G, 2CEK, 2CKM, 2DFP, 2J3D, 2J3Q, 2J4F, 2V96, 2V97, 2V98, 2VA9, 2VJA, 2VJB, 2VJC, 2VJD, 2VQ6, 2VT6, 2VT7, 2W6C, 2W9I, 2WFZ, 2WG0, 2WG1, 2WG2, 2XI4, 3GEL, 3I6M, 3I6Z, and 3M3D), and the grids of the rigid part of the *Tc*AChE structure were produced by using the energetic grid module (6) and Zou GB/SA grid models (3) encoded in DOCK6.5 (12). Of note, the centers for grids generation were consistent with the centers of the selected subboxes for binding configuration sampling. That is, one set of grids (including the energetic grid and Zou GB/SA grids) was needed to be prepared for each selected subbox. In this study, the energetic grid was defined with a size of $35 \times 35 \times 35$ Å^3 and the Zou GB/SA grids were defined with a dimension of $19 \times 19 \times 19$ Å^3 due to the limitation in the memory requirement for calculation. The degrees of protein flexibility were defined on the basis of experimental observation. For *Tc*AChE studied in this work, conformational changes were observed in the 13 residues located around the predicted tunnels, including Y70, W84, Y121, S122, E199, W279, F288, F290, F330, F331, Y334, W432, and H440. The flexibilities of these residues were considered during the binding free energy landscape (BFEL) construction.

Fitting ω_1–ω_4 Values for *Tc*AChE. The X-ray crystal structures of eight inhibitor–*Tc*AChE complexes with experimental data of quantitative binding affinity were used for fitting the values of ω_1–ω_4.

Theoretically, the more experimental data are available, the more reliable result we can obtain. However, there are only eight experimental data sets that could be used in our study. The PDB entries of these crystal structures, chemical structures of the inhibitors, and dissociation or inhabitation constants are listed in Table S1. For each inhibitor–TcAChE complex, the four MM-GBSA energy terms, ΔE_{vdw}, ΔE_{es}, ΔG_{gb}, and ΔG_{sa}, were calculated using Eqs. **S2–S5**, respectively, and the results are also listed in Table S1. These calculation data were used to fit the experimental binding free energies using the multiple linear regression method, and the optimized values of ω_1–ω_4 were obtained with a relatively high confidence ($R^2 = 0.6926$). The fitted data of ω_1–ω_4 and the linear relationship between the experimental and predicted binding free energies are shown in Fig. S2. These fitted values of ω_1–ω_4 were used in constructing the binding free energy landscape for HupA–TcAChE binding.

Molecular Docking for Binding Configurations Sampling. Docking is an obviously appropriate approach to simulate the binding models for ligand–receptor interactions at a large-scale level because of its rapid computing speed (13). Nevertheless, owing to the lack of diversity in sampled binding poses and inaccuracy for binding affinity prediction, the existing docking tools were not adequate for the construction of the BFEL. Therefore, in the present study, we used a unique docking method developed in our laboratory to simulate and sample the binding configurations. There are two key improvements of our docking method in comparison with others: (*i*) we used Eq. **S1** as a scoring function during the docking simulation, and thus the binding affinity of each binding configuration could be accurately estimated; (*ii*) with consideration of the delicate balance among Van der Waals interaction, electrostatic interaction, solvent effects, and conformational changes in ligand–receptor binding, we designed a multiobjective model to optimize the binding pose by taking the four energy terms in Eq. **S1** (ΔE_{vdw}, ΔE_{es}, ΔG_{gb}, and ΔG_{sa}) as objective functions. The multiobjective optimization was performed by using the nonsorting genetic algorithm II (NSGA2) (14). In this way, our docking method may produce diverse binding poses and calculate corresponding binding free energies simultaneously. Of note, our docking method may address the highly fluctuant and complicated energy landscape of ligand–receptor binding with many energetically similar but structurally different local minima, as has been shown in the BFEL construction for HupA–TcAChE binding in the present study. The reason our docking method can realize such a simulation is that our docking program may fix the ligand into each lattice box and search possible binding poses within each lattice box. The process is very simple; i.e., the ligand was first dragged into the center of one lattice, and the translational range of the mass of the center of the ligand was restrained within the lattice and the rotational degree of the ligand was unlimited during docking simulation. In this way, the binding conformations of the ligand could be optimized locally within a very small grid during docking, and a relatively complete configuration space for ligand–protein interaction could be obtained. On the other hand, to avoid the loss of binding configurations at the boundaries between the neighboring lattices, additional lattices of equal size are intersected in between them. On the other hand, the ligand molecule is allowed to translate and rotate freely in a lattice as long as its center of mass does not move to its neighboring lattices. This setting will also prevent the loss of binding configurations, especially the configurations located at the transition states, caused by the global convergence of the optimization method of docking.

BFEL Construction. The BFEL is constructed in a Euclidean coordinate system: The *y* axis is the distance between the mass centers of HupA at an instantaneous configuration and that of HupA at the active site, the *x* axis is the minimized root mean SD (RMSD) between the instantaneous conformation of HupA and that at the active site of TcAChE, and the *z* axis is the calculated binding free energy of each binding configuration. About 127,371 sets of primary data of binding configurations with binding free energy values were obtained from the configuration sampling for HupA–TcAChE binding and free energy calculations. The *xy* plane was divided into 500×500 mesh grids, and the scatter data of binding free energies were fitted to the grids by using the Gridfit algorithm (15) encoded in Matlab (16). The nearest-neighbor algorithm (15) was used to interpolate data points between the primarily calculated data points, and the BFEL surface was constructed on the basis of 250,000 data points (primary plus interpolated data points) by using the iterative least-squares solver method in Gridfit (15). A smoothing process was performed to smooth the primary BFEL surface with different degrees of smoothness to obtain a reasonably accurate smooth surface.

Binding Pathway Analysis. Fig. S3*A* demonstrates the procedure of the algorithm for pathway searching. The constructed 2D BFEL was first coarse-grained into 100×100 grids and allowed a point to perform grid-to-grid movement. The point might move forward, left, and right but not backward. To simplify the process, we performed the pathway searching starting from the active site, supposing the ligand binding and unbinding within the same pathway. From one grid the point moves toward only the next grid with the lowest energy among the neighboring points. For example, at grid S1, the point will move to grid S2 rather than to S2′ and S2″ because the energies of the latter two grids are higher than that of S2. In this way, the lowest-energy pathway may be addressed from the active site (global minima) to the bulk solvent.

Surface Plasmon Resonance Determination. The thermodynamic (K_D) and kinetic parameters (k_{on} and k_{off}) of HupA–TcAChE binding were determined by using surface plasmon resonance (SPR) technology. SPR measurements were performed on a BIAcore T200 instrument (BIAcore GE Healthcare). TcAChE was diluted in the acetate solution (pH 4.0) with a final concentration of 50 µg/mL, and the enzyme was immobilized to one of the measurement cells of the sensor chip surface by the standard Biacore procedure, using HBS-EP buffer [10 mM Hepes, 150 mM NaCl, 3 mM EDTA, and 0.005% (vol/vol) surfactant P20, pH 7.4] at a flow rate of 10 µL/min. The enzyme was coupled covalently to the carboxymethylated dextran of a CM5 sensor chip by amino coupling. Carboxyl groups in the immobilization matrix were first activated by treatment with a fresh mixture of 0.2 M 1-ethyl-3-(3-dimethylaminopropyl) carbodiimide hydrochloride and 50 mM *N*-hydroxysuccinimide for 7 min. The enzyme at the same concentration (50 µg/mL in 10 mM sodium acetate, pH 5.2) was then injected over the surface until a desired immobilization level [4,900 resonance units (RU)] was reached. Finally, unreacted *N*-hydroxysuccinimide esters were blocked by 1 M ethanolamine, pH 8.5, for 7 min. Binding affinity measurements were performed in a continuous flow of 30 µL/min, using HBS-EP as the running buffer. The HupA chemical was diluted in the running buffer and automatically injected in a series of increasing concentrations (0, 62.5, 125, 250, 500, 1,000, and 2,000 nM). The binding responses were recorded continuously in RU at a frequency of 1 Hz as sensorgrams and presented as a function of time (illustrated in Fig. S6*A*). Sensorgrams were processed by using automatic correction for nonspecific bulk refractive index effects. Data processing and analysis were performed using Biacore T200 evaluation software in a 1:1 binding model (BIAcore GE Healthcare Bio-Sciences).

Binding Free Energy and Activation Free Energies Derived from SPR Data. The association rate constant (k_{on}) and dissociation rate constant (k_{off}) obtained from the SPR determinations were used to obtain binding constant (K_D) and corresponding binding free energy,

$$K_D = \frac{k_{off}}{k_{on}} \qquad \text{[S6]}$$

$$\Delta G_{binding} = RT \ln K_D. \qquad \text{[S7]}$$

In principle, activation free energies for the association ($\Delta G_{on}^{\neq}$) and dissociation ($\Delta G_{off}^{\neq}$) processes could be obtained using Eyring's equation,

$$\Delta G_{on}^{\neq} = -RT \ln\left(\frac{k_{on}h}{k_B T}\right), \quad \Delta G_{off}^{\neq} = -RT \ln\left(\frac{k_{off}h}{k_B T}\right), \qquad \text{[S8]}$$

where h is the Planck constant and k_B is the Boltzmann constant. In practice, $\Delta G_{on}^{\neq}$ and $\Delta G_{off}^{\neq}$ are obtained in the following way: (*i*) Determine k_{on} and k_{off} values at several different temperatures in a range; (*ii*) fit the k_{on} and k_{off} values to the linear

form of Eyring's equation to obtain the activation enthalpy ($\Delta H_o^{\neq}$) and entropy ($\Delta S_o^{\neq}$),

$$\ln\frac{k_o}{T} = -\frac{\Delta H_o^{\neq}}{RT} + \ln\frac{k_B}{h} + \frac{\Delta S_o^{\neq}}{R}, \qquad \text{[S9]}$$

where "o" represents "on" or "off"; and (*iii*) calculate the activation free energy by

$$\Delta G_o^{\neq} = \Delta H_o^{\neq} - T\Delta S_o^{\neq}. \qquad \text{[S10]}$$

For HupA–*Tc*AChE binding, the k_{on} and k_{off} values at five different temperatures in the 10–30 °C range were determined by using SPR (Table S2). The fitted linear relationships of $\ln(k_{on}/T)$ and $\ln(k_{off}/T)$ with $1/T$ are obvious; the R^2 values are as high as 0.9991 and 0.9687, respectively (Fig. S6 *B* and *C*).

1. Still WC, Tempczyk A, Hawley RC, Hendrickson T (1990) Semianalytical treatment of solvation for molecular mechanics and dynamics. *J Am Chem Soc* 112(16):6127–6129.
2. Hawkins GD, Cramer CJ, Truhlar DG (1995) Pairwise solute descreening of solute charges from a dielectric medium. *Chem Phys Lett* 246(51):122–129.
3. Zou XQ, Sun YX, Kuntz ID (1999) Inclusion of solvation in ligand binding free energy calculations using the generalized-Born model. *J Am Chem Soc* 121(35):8033–8043.
4. Liu HY, Kuntz ID, Zou XQ (2004) Pairwise GB/SA scoring function for structure-based drug design. *J Phys Chem B* 108(17):5453–5462.
5. Hawkins GD, Cramer CJ, Truhlar DG (1996) Parameterized models of aqueous free energies of solvation based on pairwise descreening of solute atomic charges from a dielectric medium. *J Phys Chem* 100(51):19824–19839.
6. Meng EC, Shoichet BK, Kuntz ID (1992) Automated docking with grid-based energy evaluation. *J Comput Chem* 13(4):505–524.
7. Shoichet BK, Kuntz ID, Bodian DL (1992) Molecular docking using shape descriptors. *J Comput Chem* 13(3):380–397.
8. Shelley JC, et al. (2007) Epik: A software program for pK_a prediction and protonation state generation for drug-like molecules. *J Comput Aided Mol Des* 21(12):681–691.
9. Gasteiger J, Marsili M (1980) Iterative partial equalization of orbital electronegativity—a rapid access to atomic charges. *Tetrahedron* 36(22):3219–3228.
10. Tripos (2001) SYBYL (Tripos, St. Louis), Version 6.8.
11. Wang JM, Cieplak P, Kollman PA (2000) How well does a restrained electrostatic potential (RESP) model perform in calculating conformational energies of organic and biological molecules? *J Comput Chem* 21(12):1049–1074.
12. Lang PT, et al. (2009) DOCK 6: Combining techniques to model RNA-small molecule complexes. *RNA* 15(6):1219–1230.
13. Garrett MM, Marguerita L-W (2008) *Molecular Modeling of Proteins*, ed Andreas K (Humana Press, New York), pp 365–382.
14. Kanpur PA, Agarwal S, Meyarivan T (2002) A fast and elitist multiobjective genetic algorithm: NSGA-II. *IEEE Trans Evol Comput* 6(2):182–197.
15. Keim DA, Herrmann A (1998) The *Gridfit* algorithm: An efficient and effective approach to visualizing large amounts of spatial data. *Proceedings of IEEE Visualization, 1998. International Conference on 24 October 1998*, eds Banissi E, Khosrowshahi F, Sarfraz M (IEEE Computer Society Press, Los Alamitos, CA), pp 181–188.
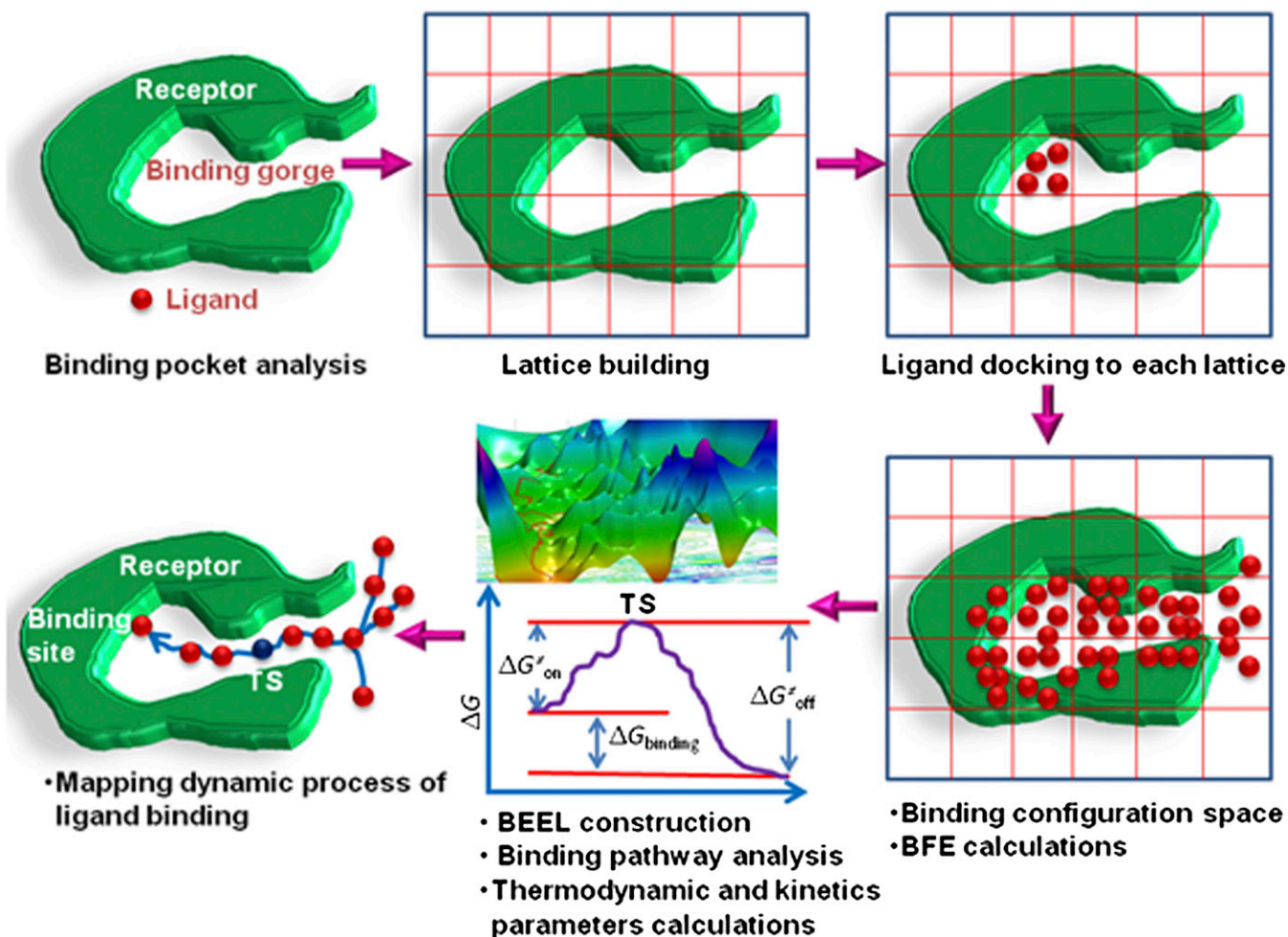16. The Mathworks (2009) MATLAB (The Mathworks, St. Natick, MA), Version 7.9.0 (R2009b).

Fig. S1. Work flow of construction of binding free energy landscape (BFEL) for the ligand–receptor binding process: (*i*) Analyze the binding pocket properties and define the flexible residues for following docking simulations and MM-GBSA calculations. (*ii*) Divide the binding pocket of receptor into sub cubics (lattices). (*iii*) Dock the ligand into each lattice and obtain the binding configurations located inside the lattice. During docking simulations, a multiobjective optimization algorithm developed in our laboratory is used to obtain the binding poses of the ligand by taking the four energy terms in Eq. **S1** as objective functions (*SI Text*). (*iv*) Construct binding configuration space by taking together the docking data of all lattices. (*v*) Construct the BFEL on the basis of the information of the binding configuration space, including ligand–receptor complex structures and binding free energies of the points in the binding configuration space. Search the possible binding pathway of ligand to protein from the BFEL, and calculate binding free energy and activation free energies for the association and dissociation processes. (*vi*) Map the structure snapshots of ligand–receptor binding to the binding pathway; obtain the structural information of possible stable states, metastable states, and transition states for the ligand binding to the receptor; and propose possible mechanisms for ligand binding.
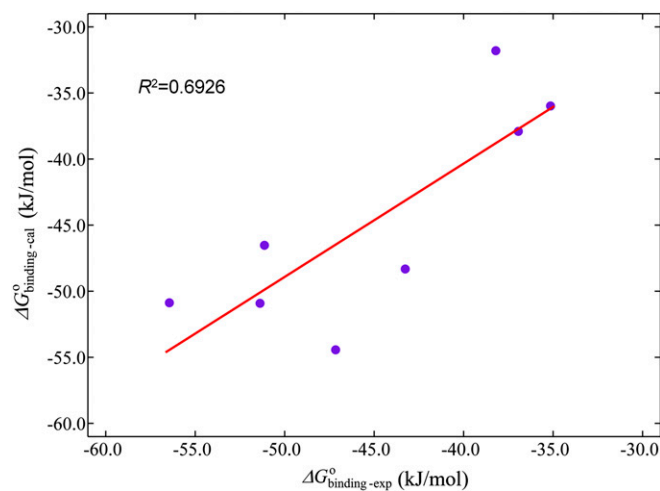
$R^2 = 0.6926$

Fig. S2. Linear relationship between the experimental and predicted binding free energies calculated using the improved MM-GBSA method for the eight available inhibitors binding to *Tc*AChE (Table S1).
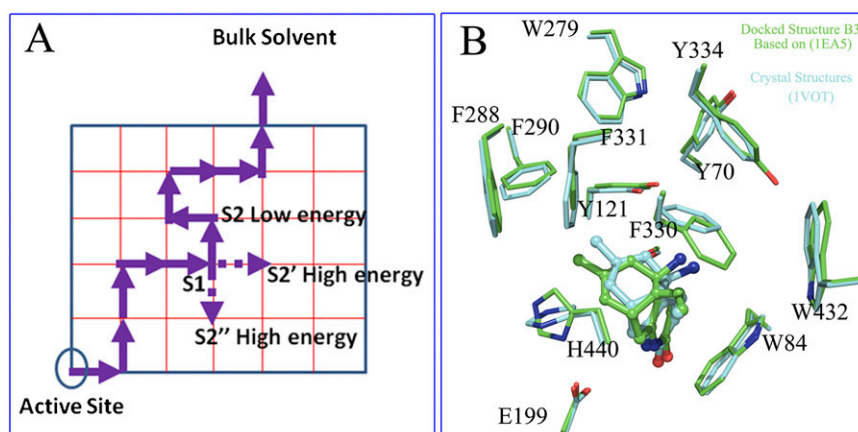

Fig. S3. (*A*) Schematic representation of the grid-to-grid unbinding pathway searching algorithm. Starting from the grid of the active site, the ligand moves toward the next grid with the lowest energy among the neighboring points. (*B*) Comparison of the docking-derived binding configurations of HupA to *Tc*AChE (at the B3 state) with the X-ray crystal structure of the HupA–*Tc*AChE complex (PDB ID: 1VOT). Only the residues around the active site are shown. The carbon atoms of HupA and residues of *Tc*AChE in the X-ray structure are colored in cyan and the atoms in the docked structure are colored in green, respectively. HupA is shown in a ball-and-stick model, and the residues are shown as sticks. The docked configuration of HupA agreed well with the crystal structure with an RMSD of 0.588 Å, and the docked conformation of flexible residues of *Tc*AChE agreed with the crystal structure with an RMSD of 0.775 Å.
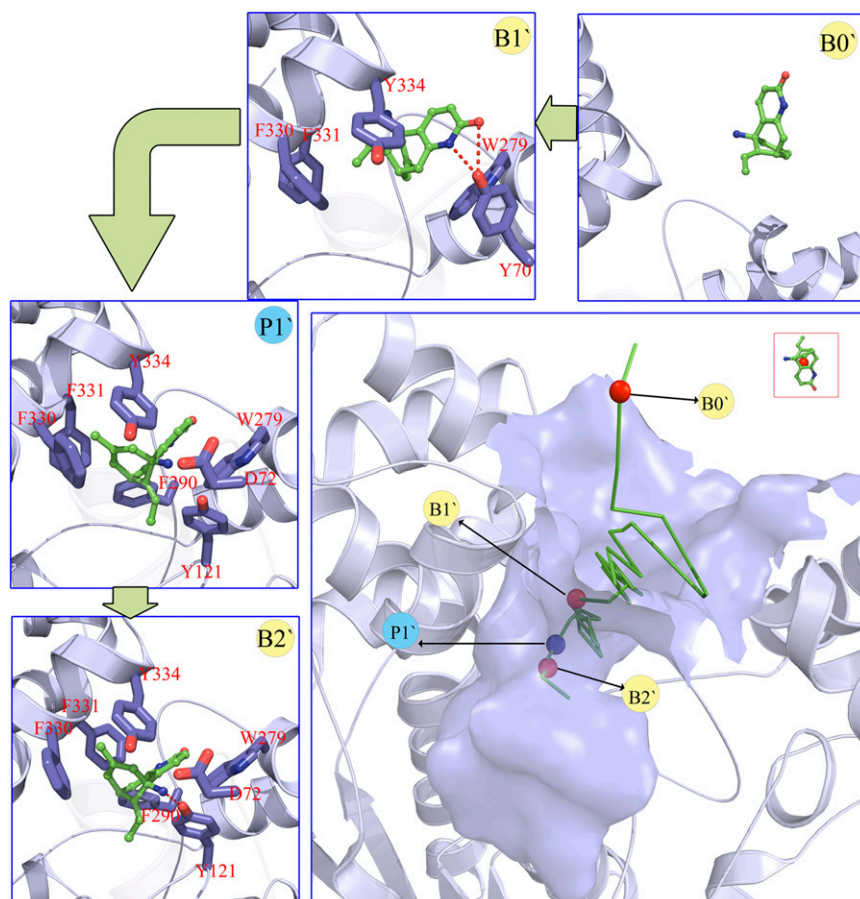
Fig. S4. Structural features of the alternative possible binding pathway of HupA entering into the gorge of *Tc*AChE. (*Lower Right*) Binding pathway of HupA to *Tc*AChE corresponding to the binding free energy profile shown in Fig. 3. Green stick reflects the lowest binding free energy pathway portrayed by the centers of mass of the instantaneous conformations of HupA. Balls indicate the (meta)stable states (red) and transition states (blue). Smaller panes (*Upper* and *Left*) represent Interaction models for the metastable, stable, and transition states indicated in the binding pathway. Red dashed lines in structural models indicate the hydrogen bonds.
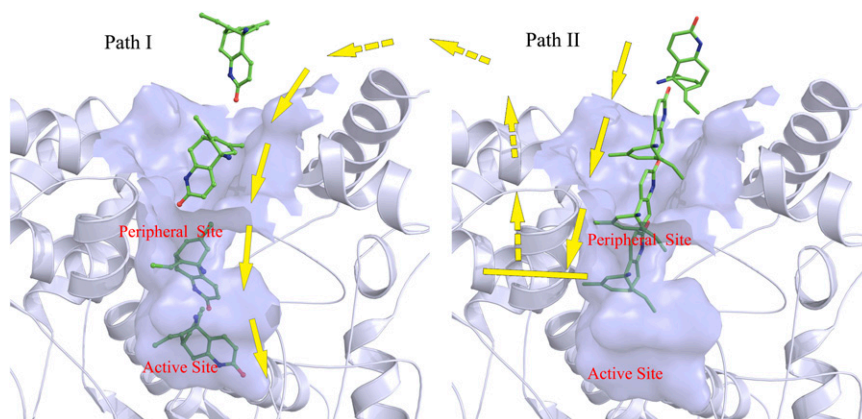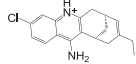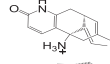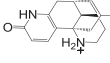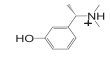

Fig. S5. Two possible binding orientations for HupA entering the active gorge of *Tc*AChE. Through path I (*Left*), HupA could reach the active site. HupA could arrive only at the bottom of the peripheral anionic site and could not move farther to reach the active site via path II (*Right*).

Fig. S6. (*A*) Surface plasmon resonance (SPR) sensorgrams of the binding of HupA to *Tc*AChE. SPR determination for the binding of HupA with *Tc*AChE is shown. Real-time binding measurements of HupA to *Tc*AChE at five different temperatures (283.15, 288.15, 293.15, 298.15, and 303.15 K) were performed by using a BIAcore T200 instr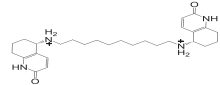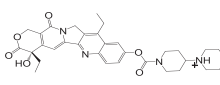ument (BIAcore GE Healthcare). Representative sensorgrams were obtained from injections of HupA at concentrations of 62.5, 125, 250, 500, 1,000, and 2,000 nM (curves from top to bottom) at each temperature. HupA was injected for 180 s for association, and dissociation was monitored for more than 360 s. (*B* and *C*) Eyring plots of the association (*B*) and dissociation (*C*) rate constants for HupA–*Tc*AChE binding. The rate constants were from the SPR determinations at five different temperatures (*A* and Table S2).

Table S1. Chemical structures and experimental binding affinities of AChE inhibitors used for fitting the values of ω_1–ω_4 in Eq. 1 and the MM-GBSA calculation results of these inhibitors binding to TcAChE

PDB ID codes	Inhibitors	K_D, nM*	$\Delta G_{\text{binding-exp}}$, kJ/mol†	ΔE_{vdw}, kJ/mol	ΔE_{es}, kJ/mol	ΔG_{gb}, kJ/mol	ΔG_{sa}, kJ/mol	$\Delta G_{\text{binding-cal}}$, kJ/mol
1E66		0.13 (1)	−50.88	−190.78	−423.43	505.02	17.18	−52.50
1GPK		175 (2)	−31.76	−149.42	−123.80	216.83	9.46	−34.67
1GPN		334 (1)	−37.91	−164.17	−165.05	247.86	16.17	−41.28
1GQR		700 (1)	−37.21	−57.42	37.07	20.40	27.60	−34.71
1H22		0.8 (3)	−50.91	−254.35	−102.36	180.79	18.89	−45.66
1H23		4.5 (3)	−54.42	−270.33	−158.12	266.23	19.92	−53.84
1U65		26.4 (3)	−48.32	−190.37	−479.24	528.88	12.41	−45.43
2CKM		0.077 (4)	−46.53	−266.59	−217.06	320.74	14.29	−50.09

*Experimental dissociation constants from refs. 1–4 (reference numbers in parentheses).
†Binding free energies calculated from the binding constants by relation of $\Delta G_{\text{binding-exp}} = RT \ln K_D$.

1. Dvir H, et al. (2002) 3D structure of Torpedo californica acetylcholinesterase complexed with huprine X at 2.1 A resolution: Kinetic and molecular dynamic correlates. *Biochemistry* 41(9): 2970–2981.
2. Wong DM, et al. (2003) Acetylcholinesterase complexed with bivalent ligands related to huperzine a: Experimental evidence for species-dependent protein-ligand complementarity. *J Am Chem Soc* 125(2):363–373.
3. Butini S, et al. (2008) Exploiting protein fluctuations at the active-site gorge of human cholinesterases: Further optimization of the design strategy to develop extremely potent inhibitors. *J Med Chem* 51(11):3154–3170.
4. Rydberg EH, et al. (2006) Complexes of alkylene-linked tacrine dimers with Torpedo californica acetylcholinesterase: Binding of Bis5-tacrine produces a dramatic rearrangement in the active-site gorge. *J Med Chem* 49(18):5491–5500.

Table S2. SPR data for HupA–TcAChE binding at five different temperatures

T, K	k_{on}, M$^{-1} \cdot$s^{-1}	k_{off}, s^{-1}	K_D, M^{-1}	χ^2, RU^2
283.15	3.38×10^3	1.80×10^{-3}	5.32×10^7	6.00×10^{-3}
288.15	6.98×10^3	2.30×10^{-3}	3.29×10^7	9.00×10^{-3}
293.15	1.36×10^4	3.52×10^{-3}	2.58×10^7	1.43×10^{-2}
298.15	2.65×10^4	5.67×10^{-3}	2.14×10^7	1.10×10^{-2}
303.15	4.53×10^4	8.01×10^{-3}	1.77×10^7	4.20×10^{-2}